NUMERICAL COMPUTATION OF HEAT TRANSFER ON REENTRY CAPSULES AT MACH 5

R.C. Mehta*

Abstract

The heat transfer over various reentry axisymmetric configurations is studied numerically by solving time-dependent compressible laminar Navier-Stokes equations. The governing fluid flow equations are disrectized in spatial coordinates employing a finite volume approach, which reduces the equations to semi-discretized ordinary differential equations. Temporal integration is performed using multi-stage Runge-Kutta time stepping scheme. A local time step is used to achieve steady state solution. The numerical simulation is carried out on a mono-block structured grid. The numerical computation is carried out for freestream Mach number of 5.0. The numerical scheme captures well all the essential flow field features such as bow shock wave, sonic line, expansion fan on the corner, recompression shock wave and recirculating flow in the base region. Comparisons of the flow field, surface pressure, skin friction coefficient and wall heat flux results are made between different configurations of the reentry capsules such as ARD (ESA's Atmospheric Reentry Demonstrator), CARINA, Apollo, Muses-C (Mu Science Engineering Satellite), OREX (Orbital Reentry Experiments) and Beagle-2. The effects of geometrical parameters of the different reentry capsules on surface pressure, skin friction coefficients and heat flux and forebody aerodynamic drag are analyzed. Base pressure is independent of the forebody shape of the reentry capsules. The effects of module geometry on the flow field are numerically analyzed which may be useful for optimization of the reentry capsule.

Introduction

A high-speed flow past a blunt body generates a bow shock wave which causes a rather high surface pressure and as a result the development of high aerodynamic drag which is needed for decelerating or aerobraking of reentry capsule. Most current aero-thermodynamic designs feature a blunt forebody shielding the payload from the intense heat generated during atmospheric reentry. One of the important design parameters in the design of the reentry capsule is trade off between its weight and reentry velocity. A low mass-to-drag ratio is often selected for reentry module. The design approach of the reentry capsule needs a high drag with good static stability margin, which leads to the selection of an axisymmetric spherically blunt configuration. The nose radius is selected for minimum structural mass with maximum drag, leading to a maximized radius limited by the large range of bluntness ratio. Highly spherically blunt or combination of spherical-nose with cone fore body configuration generally preferred for aerobraking of reentry capsule for safe returning on the Earth after performing the experiment in the space.

The features of flow field over the reentry capsule can be delineated through the experimental investigations at high speeds that can be described by following. The bow shock wave is detached from the blunt fore body and is having a mixed subsonic-supersonic region between them. Fig.1 shows schematic features of the flow field over reentry body. In the fore body region the fluid strongly decelerates through the bow shock wave, and high-pressure, temperature, and density generated depending upon the reentry speed and altitude of the returning capsule. At the shoulder, the flow turns and expands rapidly, and boundary layer detaches, forming a free shear layer that separates the inner recirculating region behind the base from the outer flow field. The latter is recompressed and turned back to freestream direction, first by the so-called slip flow, and further downstream by recompression shock. At the end of the recirculation past the neck, the shear layer develops in the wake trail. A complex inviscid wave structure often includes a lip shock (associates with the corner expansion) and a wake shock (adjacent to the shear layer confluence). The flow field over the reentry configurations became further complex due to the pres-

* Scientist/Engineer, Aerodynamics Division, Vikram Sarabhai Space Centre, ISRO Post, Thiruvananthapuram-695 022, India
Manuscript received on 23 Aug 2005; Paper reviwed, revised and accepted on 02 May 2006

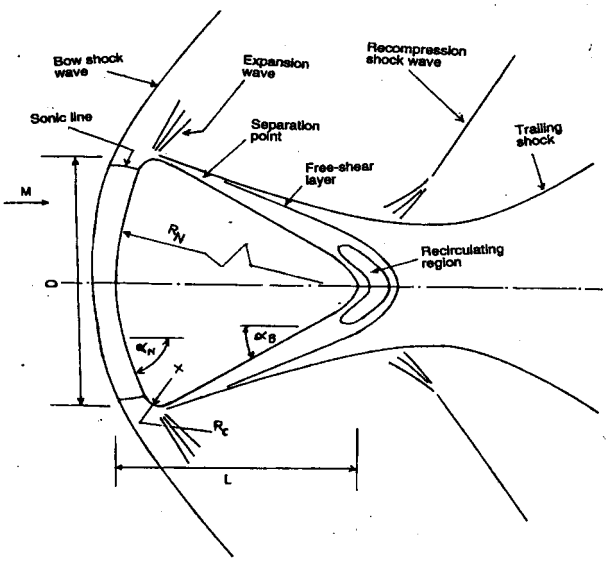

Fig.1 Representation of flow features on the blunt body at supersonic speeds

ence of the corner at the shoulder and the base region of the module. The corner expansion process is a modified Prandtl-Mayer pattern distorted by the presence of the approaching boundary layer. As the flow breaks away from the base plane it is brought to the base pressure by a weak shock wave known as the 'lip shock' downstream from the lip shock, the free shear layer begins to form. A free shear layer (in contrast to a boundary layer) is characterized by nearly zero velocity derivatives (shear stresses) at each edge of the layer. In contrast to the base pressure, the relative low velocity adjacent to the base plane significantly affects the level of base plane heat convection.

A large number of computational fluid dynamics simulations [1-6] have been performed for aerobraking and reentry capsules. The numerical solution of Navier-Stokes equations in the near wake region of the reentry module is carried out by Allen and Cheng [4], which confirms the mechanism of flow separation as, observed experimentally [5]. Base drag represents the loss in recovery of pressure over the base of the capsule [7]. The supersonic and hypersonic laminar flow over a slender cone has been numerically calculated by Tai and Kao [8]. A summary of developments relating to the base pressure prediction is reported in the review paper of Lamb and Oberkamf [9]. An aerodynamic analysis of the Commercial Experiment Transport (COMET) reentry capsule has been carried by Wood et al. [10] solving the laminar thin layer Navier-Stokes equations flow solver LAURA. The flow field past blunt and short reentry capsule has been analyzed in order to understand the mechanism of the instability at supersonic speeds, which occurs due to decay of base pressure [11]. Yamamoto and Yoshioka [12] have computed flow field over OREX reentry module in conjunction with the in-depth thermal analysis of thermal protection system and results were compared with the flight data. Tam [13] has used LUSGS implicit scheme for flow computation over On-Axis Biconic and Aeroassist Flight Experiment (AFE) reentry vehicles. Liever et al. [14] solved the flow field over Beagle reentry capsule. The flow field and the heat flux computation over the Mars pathfinder vehicle has been numerically carried out by Haas and Venkatapathy [15] along with fore body and wake flow structure during atmospheric entry of the spacecraft. In many cases geometrical simplifications of configurations used for Computational Fluid Dynamics evaluation introduces errors in aerodynamic quantities comparable than those arising from numerical accuracy or lack of physical modeling of the respective code [16]. Following the completion of the Exploration Architecture Study System (ESAS) [17], NASA chose a blunt-body capsule as the Crew Exploration Vehicle (CEV) reentry module that is having similar shape of the Apollo command module. The CAINA module is an Apollo-Gemini like capsule whereas the ARD (Atmospheric Reentry Demonstrator) fore body design is geometrically identical to the fore body shape of the Apollo entry capsule. It is noticed from various reentry capsule configurations that the large nose radius of the reentry capsule is preferred in order to obtain large aerodynamic drag.

In the present work, numerical studies were undertaken for a freestream Mach number of 5.0 for the numerical simulation to solve axisymmetric laminar compressible unsteady Navier-Stokes equations is carried out employing two-stage Runge-Kutta time-stepping scheme. The numerical scheme is second order accurate in space and time. A local time stepping is used to achieve steady state solution. The objective of the present study is to compute surface pressure, skin friction coefficient and wall heat flux and forebody aerodynamic drag on the ARD (Atmospheric Reentry Demonstrator), CARINA, Apollo, Muses-C (Mu Science Engineering Satellite), OREX (Orbital Reentry Experiments) and Beagle-2 for Mach 5. The effects of module geometry on the flow field are numerically analyzed which may be useful for optimization of the reentry capsule.

Problem Definition and Approach

Governing fluid equations

The time-dependent axisymmetric compressible Navier-Stokes equations are written in following strong conservation form, the ideal gas law for solution augments the system of equations.

$$\frac{\partial U}{\partial t}+\frac{\partial F}{\partial x}+\frac{\partial G}{\partial r}+H=\frac{\partial R}{\partial x}+\frac{\partial S}{\partial r} \tag{1}$$

where

$$U=r\begin{bmatrix}\rho\\ \rho u\\ \rho v\\ \rho e\end{bmatrix},$$

$$F=r\begin{bmatrix}\rho u\\ \rho uu+p\\ \rho uv\\ (\rho e+p)u\end{bmatrix},$$

$$G=r\begin{bmatrix}\rho v\\ \rho uv+p\\ \rho vv\\ (\rho e+p)v\end{bmatrix}$$

are the state vector **U** and inviscid flux vector **F** and **G**. The viscous vectors **R**, **S** and **H** are

$$R=r\begin{bmatrix}0\\ \sigma_{xx}\\ \tau_{xr}\\ u\sigma_{xx}+v\sigma_{rx}+q_x\end{bmatrix},$$

$$S=r\begin{bmatrix}0\\ \tau_{xr}\\ \sigma_{rr}\\ u\tau_{xr}+v\sigma_{rr}+q_r\end{bmatrix},$$

$$H=\begin{bmatrix}0\\ 0\\ \sigma+\\ 0\end{bmatrix}$$

where σ_{xx}, σ_{rr} and σ_{+} are components of the stress vector, q_x,q_r are components of the flux vector, u and v are axial and radial velocity components in x and r directions, respectively, e is total energy per unit volume. Thus, the viscous terms in the above equations become

$$\sigma_{xx}=-\frac{2}{3}\mu\nabla.U+2\mu\frac{\partial u}{\partial x}$$

$$\sigma_{xr}=-\frac{2}{3}\mu\nabla.U+2\mu\frac{\partial v}{\partial x}$$

$$\tau_{xr}=\tau_{rx}=\mu\left(\frac{\partial u}{\partial r}\right)+\mu\left(\frac{\partial v}{\partial x}\right)$$

$$\sigma_{+}=-p-\frac{2}{3}\mu\nabla U+2\mu\frac{v}{r}$$

$$\nabla.U=\frac{\partial u}{\partial x}+\frac{\partial v}{\partial r}+\frac{v}{r}$$

$$q_x=-\frac{Cp\mu}{Pr}\frac{\partial T}{\partial x}$$

$$q_r=-\frac{Cp\mu}{Pr}\frac{\partial T}{\partial r}$$

The flow is assumed to be laminar, which is consistent with the numerical simulation of [8,10,11,18]. The coefficient of molecular viscosity is computed according to Sutherland's law as

$$\mu=1.458\times10^{-6}\frac{T^{1.5}}{T+110.4} \tag{2}$$

The temperature T is related to the pressure p and density ρ by the perfect gas equation of state as

$$\frac{p}{(\gamma-1)}=\left[\rho e-\frac{1}{2}\rho(u^2-v^2)\right] \tag{3}$$

The ratio of specific heats γ was assumed constant and equal to 1.4.

Numerical Algorithm

The flow field code employs a finite volume discretization technique. Using a finite-volume approach, the governing equations are discretized in space starting from an integral formulation and without any intermediate mapping. The spatial computational domain is divided into number of non-uniform and non-overlapping quadrilateral grids. A cell centre scheme is used to store the flow

variables. On each cell face the convective and diffusive fluxes are calculated after computing the necessary flow quantities are obtained by a single averaging of adjacent cell-centre values of dependent variables [19]. The numerical procedure reduces to central differencing on a rectangular and smooth grid. The entire spatial discretization scheme is second order accurate. In viscous calculations, the dissipative properties are present due to diffusive terms. Away from the shear layer regions, the physical diffusion is generally not sufficient to prevent the odd-even point decoupling of centered numerical schemes. Thus, to maintain numerical stability and to prevent numerical oscillations in the vicinity of shocks or stagnation points, artificial dissipation terms [20] are included as blend of a Laplacian and biharmonic operator in a manner analogous to the second and fourth differences. Artificial dissipation terms are added explicitly to prevent numerical oscillations near shock waves to damp high frequency undamed modes.

Temporal integration is performed using two-stage Runge-Kutta time stepping scheme of Jameson et al. [20]. The artificial dissipation terms are evaluated only at the first-stage. The two-stage Runge-Kutta time-stepping method has been second order accurate in time for a linear system of one-dimensional equations. A conservative choice of the Courant-Friedritchs-Lewy (CFL) number 0.8 is made to obtain stable numerical solution. A local time-step is used to obtain steady-state solution.

Initial and Boundary Condition

Conditions corresponding to freestream Mach number of 5 and an altitude of 29 km are given as an initial condition. The initial values of pressure, density and temperature are 1325 Pa, 0.02125 kg/m^3 and 231 K, respectively.

The boundary conditions are as follows. All variables are extrapolated at the outer boundary, and no-slip condition is used as wall boundary condition. An isothermal wall condition has been considered for the surface of the reentry configuration. The wall temperature is prescribed as 231 K. A symmetry condition is applied on the centre line ahead and downstream of the reentry capsule.

Geometrical Details of Reentry Modules

The dimensional details are mentioned in Fig.1 where D is maximum diameter of the capsule, R_N is the spherical radius, the corner radius is R_C, α_N is the semi-cone angle, α_B is back-shell angle. The overall length of the module is L. The dimensional details of the ARD, Apollo, OREX, CARINA, MUSES-C and Beagle-2 are depicted in Fig. 2. Table-1 gives the numerical values of the geometrical parameters of the various reentry capsules.

Computational Grid

One of the controlling factors for the numerical simulation is proper grid arrangement. In order to initiate the numerical simulation of flow along the reentry module, the physical space is discretized into non-uniform spaced grid points. These body-oriented grids are generated using a finite element method in conjunction with homotopy scheme. The typical computational space of the reentry module is defined by a number of grid points in cylindrical coordinate system. Using these surface points as the reference nodes, the normal coordinate is then described by exponentially structured field points, extending onwards upto an outer computational boundary. The stretching of grid points in the normal direction is obtained using exponentially stretching relation. These grids are generated in

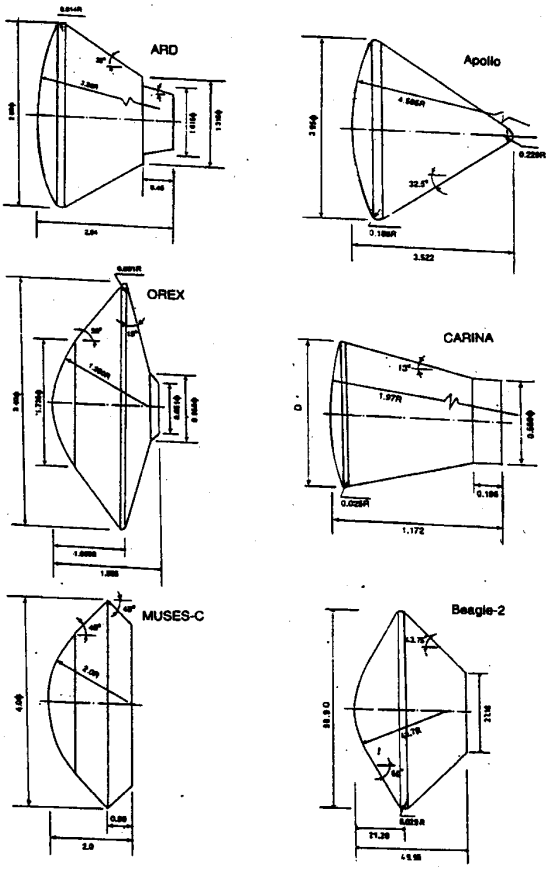

Fig.2 Dimensional detail of the reentry modules

Table-1 : Geometrical parameters of reentry capsules

Capsule	Spherical radius, R_N	Frontal diameter, D	Corner radius, R_C	Overall length, L	Semi-cone angle, $\alpha_{N\ deg}$	Back-shell angle $\alpha_{B\ deg}$
ARD	3.36	2.80	0.014	2.04	-	33.0
Appolo	4.595	3.95	0.186	3.52	-	33.0
OREX	1.35	3.40	0.01	1.50	50	75.0
CARINA	1.97 D	1.0D	0.25 D	1.172 D	-	13.0
MUSES-C	2.0	4.0	-	2.0	45	45.0
Beagle-2	41.7	90.0	0.029	49.95	60	43.75

an orderly manner. Grid independence tests were carried out, taking into consideration the effect of the computational domain, the stretching factor to control the grid intensity near the wall, and the number of grid points in the axial and normal directions [21]. The outer boundary of the computational domain is varied from 1.5 to 5. The present numerical analysis is carried out on 132x62 grid points. Fig.3 displays the enlarged view of the mono-block structured grid over various reentry configurations. This spatial resolution is adequate for fine resolution of the boundary layer and complex flow field. The finer mesh near the wall helps to resolve the viscous effects. The coarse grid helps reducing the computer time. The grid-

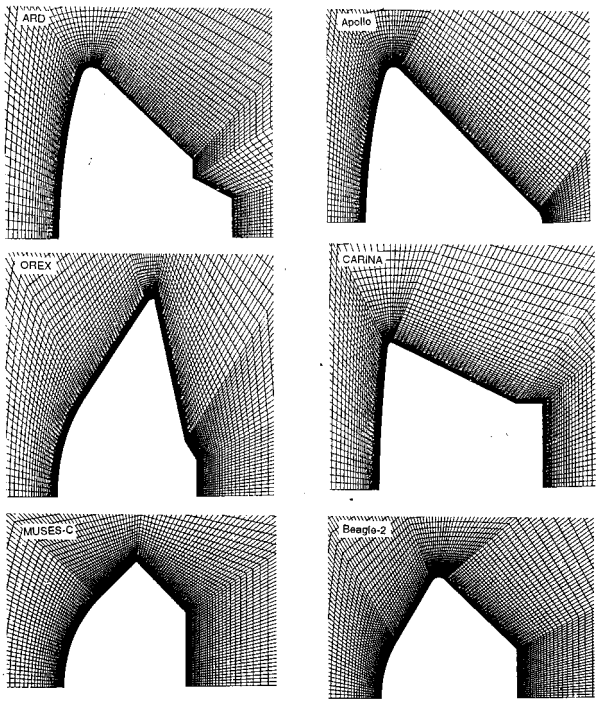

Fig.3 Enlarged view of grid arrangement over the reentry modules

s

tretching factor is selected as 5, and the outer boundary of the computational domain is maintained as 4-5 times maximum diameter of the reentry module. In the downstream direction the computational boundary is about 6-10 times diameter of the module. The grid arrangement is found to give a relative difference of about ±1.5% in the computation of drag coefficient [22]. The convergence criterion is based on the difference in density values ρ at any grid points between two successive iterations $|\rho^{n+1} - \rho^{n}| \le 10^{-5}$ where *n* is iteration index.

Results and Discussion

The numerical method describes in the previous section is applied to compute flow field over ARD (Atmospheric Reentry Demonstrator), CARINA, Apollo, Muses-C (Mu Science Engineering Satellite), OREX (Orbital Reentry Experiments) and Beagle-2 for freestream Mach 5 and freestream Reynolds number of 2.1579×10^{6}/m.

Flow Characteristics

Figure 4 shows the closed view of the velocity vector plots on various reentry capsules at Mach number, M=5.0. It can be seen from the vector plots that the bow shock wave follows the body contour relatively closely to the forebody. The formation of the bow shock wave on the fore body of the capsule is observed, which depends on R_N and α_N. A gradual flow turning can be visualized in the case of ARD, OREX, Apollo, CARINA and Beagle-2 whereas a sharp flow turning is found in the sharp shoulder edge of Muses-C. A separated flow can be observed in the base region of the reentry capsule. The flow around the capsule is divided into regions inside and outside of the recirculation, and the shear layer separates two regions. The flowfield is very complex because of the back-shell geometry.

The Mach number contour plots in Fig.5 depicts the overall flowfield structure. Characteristic features of the flow field around the blunt body at supersonic speeds, such as bow shock wave ahead of the capsule, the wake, and the recompression shock waves emanating from the neck point, are observed in the Mach contours. The bow shock wave follows the body contour and the fore body is entirely subsonic up to the corner tangency point of reentry capsule where the sonic line is located. Rapid expansion around the forebody corner produces high Mach numbers in the outer inviscid region of the wake. After the forebody corner, the boundary layer separates from the after body of the vehicle to from a free shear layer, which reattaches to the downstream of the base of the vehicle. These flow field features can also be seen in the velocity vector plots of Fig.4. The flow within the recirculation vortex formed between the free shear layer and wall remains subsonic, while the velocity within the free shear layer varies from roughly subsonic at the inner edge to supersonic at the outer edge. The flow expands at the base corner and its followed by the recompression shock downstream of the base which realigns the flow. The flow then develops in the trailing wake. The nose is truncated before complement of local inclination at the spherical body of 45 deg, 50 deg. and 60 deg. in the cases of Muses-C, OREX and Beagle-2, respectively, the sonic point moves to the corner, changing the flow over the entire spherical cap of ARD, Apollo and CARINA. The changes in the inviscid flow field propagate throughout the subsonic region. Fig.6 gives temperature contours over different reentry modules. The temperature on the fore body of the capsule is very high as compared to base region. The supersonic wake field immediately behind the capsule base exhibits complex flow characteristics and requires a quantitative analysis of the flow field. A supersonic reentry body leaves behind a long trail of hot air.

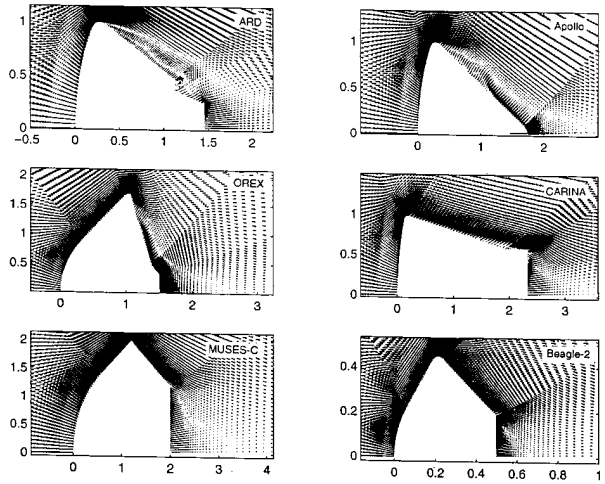

Fig.4 Vector plots over various reentry modules

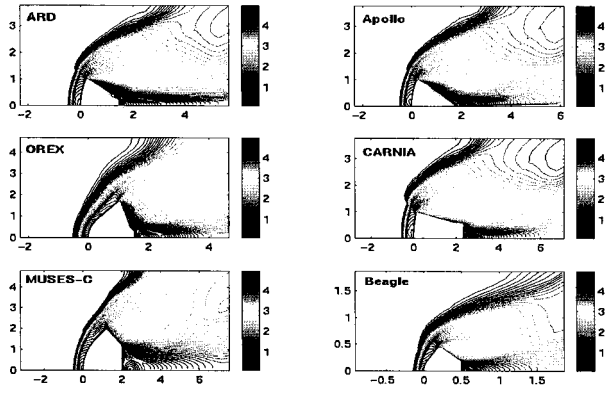

Fig.5 Mach contours over reentry modules at M=5.0

Wall Quantities

In this section, the variations of the surface quantities such as surface pressure, skin friction and heat flux are analyzed for different type of reentry capsule. The surface pressure coefficient C_p is calculated along the capsule using the following expression

$$C_p = \frac{(p - p_\infty)}{0.5\rho_\infty u_\infty^2} \tag{4}$$

where ∞ represents the freestream condition. The s/D = 0 location is the stagnation point, where *s* is the distance measured along the surface from the stagnation point and D is the maximum diameter of the capsule. Fig. 7 displays the surface pressure coefficient variation along the model

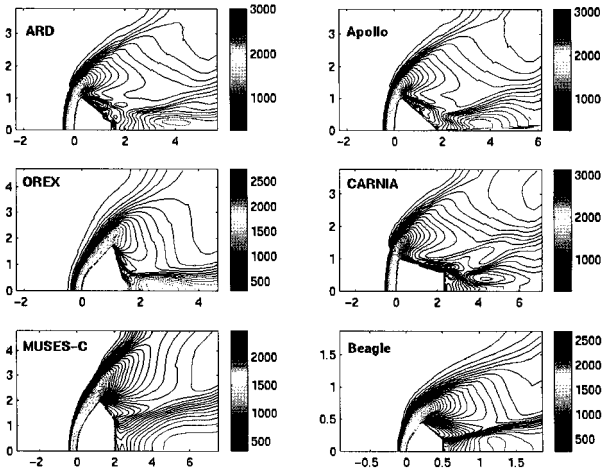

Fig.6 Temperature contours over reentry modules at M=5.0

surface, *s*. The OREX, Muses-C and Beagle-2 are having higher pressure as compared to ARD, Apollo and CARINA modules. The variation of pressure coefficient on the spherical region decreases gradually whereas in the conical region at remains constant. The surface pressure coefficient variation depends on the geometry of the capsules. The base pressure is constant in all the cases considered here. The variation of skin friction coefficient, C_f is shown in Fig.8. The skin friction coefficient increases in the spherical region. The skin friction coefficient drops suddenly on the corner as surface pressure coefficient drops. This may be attributed to sudden expansion of the flow on the corner. Negative skin friction can be seen on the base, which is due to separation. The heat flux distributions are depicted in Fig.9 along the surface of the

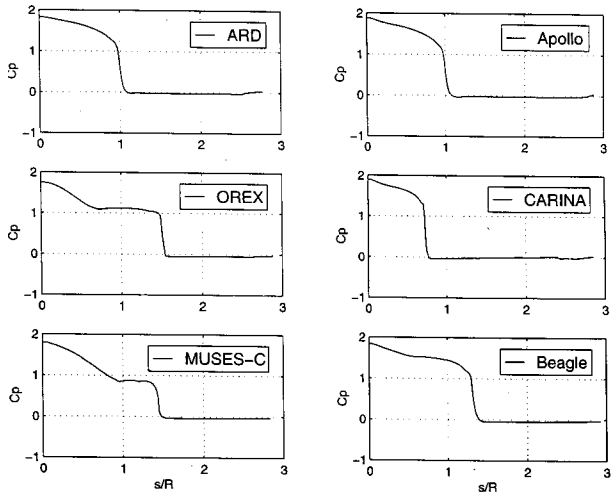

Fig.7 Pressure coefficient over the surface of the reentry capsules

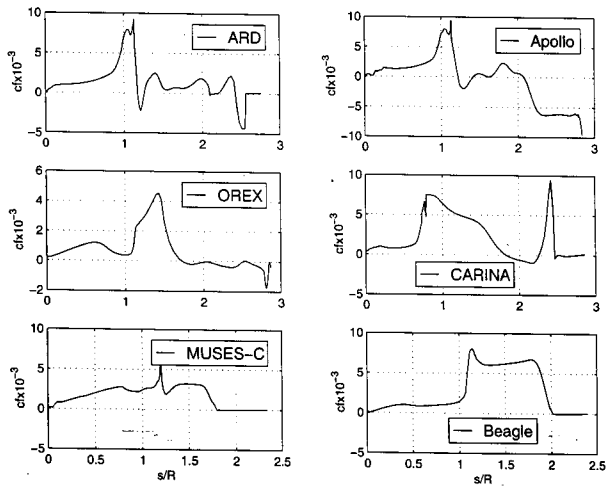

Fig.8 Skin friction coefficient over the reentry capsules

various reentry capsules. Heat fluxes present high level at the stagnation point and decrease along the front shield and second peak can be observed around the corner due to expansion of the flow. The drop of the pressure near the corner generates second heat flux peak and levels are below the stagnation point. On the back cover, the heat fluxes are smaller compare to front shield level with a maximum at 0.78 W/cm^2 on the Apollo command module which about 5% of the stagnation point heat flux value. The heat flux remains constant in the conical region of the forebody.

Aerodynamic Drag

Pressure drag is calculated by integrating the surface pressure distribution on the fore body surface that is excluding the base of the capsule. The aerodynamic drag is computed using the following expression

$$C_D = \frac{2\pi r r_i \, C_p \int (\tan\theta)_i \, dx}{A_{\max}} \tag{5}$$

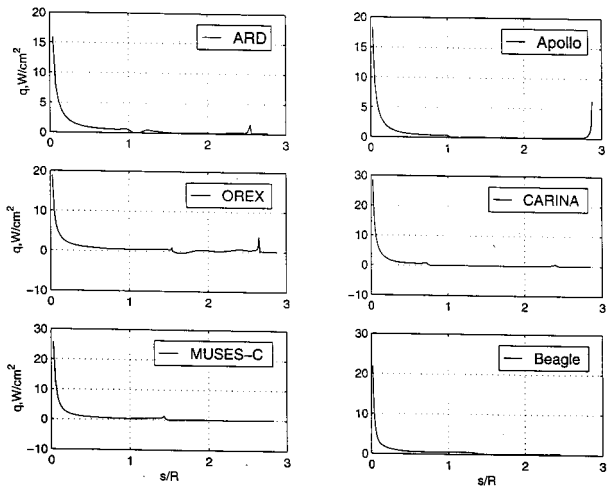

Fig.9 Surface heat flux over the reentry capsules

Table-2 : Forebody aerodynamic drag	
Capsule	C_D
ARD	1.38
Appolo	1.40
OREX	1.16
CARINA	1.45
MUSES-C	1.03
Beagle-2	1.42

where r and θ are local radius and local inclination angle in the x-direction station i. A_{max} is the maximum cross-section area of the capsule. The fore body aerodynamic drag C_D is given in Table-2 ARD, CARINA, Apollo, Muses-C, OREX and Beagle-2 for freestream Mach 5 and Reynolds number of 2.1579×10^6/m. The aerodynamic drag is greater then one for all the capsules consider in the present analysis.

Conclusion

Flow field over the reentry capsules is computed by solving compressible, laminar, axisymmetric Navier-Stokes equation. A mono-block-structured, axisymmetric, finite volume code solves the governing fluid dynamics equations using two-stage Runge-Kutta time stepping scheme with local time-stepping to accelerate convergence to a steady state. Flow fields over ARD (ESA's Atmospheric Reentry Demonstrator), CARINA, Apollo, Muses-C (Mu Science Engineering Satellite), OREX (Orbital Reentry Experiments) and Beagle-2 are computed. All the essential flow field features are fairly well captured such as bow shock wave, expansion on the corner, recompression shock wave and recirculation flow in the base region. Surface pressure and skin friction coefficients and wall heat flux distributions and fore body aerodynamic drags for various the reentry configurations are computed numerically. They are function of the geometrical parameters of the capsules. Highly spherically blunt or combination of spherical nose with cone fore body configuration generally preferred for aerobraking reentry capsule for safe returning to the Earth after performing the experiment in the space.

References

1. Gnoffo, P.A., Price, J.M. and Braum, R.D., "On the Computation of Near Wake", Aerobrake Flow Fields, AIAA Paper 91-1371, June 1991.

2. Grasso, F. and Marinir, M., "Solution of Hypersonic Flows with Total Variation Diminishing Multigrid Techniques", Computer and Fluids, Vol. 23, No. 5, 1995, pp. 571-592.

3. Venkatapathy, E., Palmer, G., and Prabhu, D.K., "AFE Base Computations", AIAA Paper 91-1372, June 1991.

4. Allen, J.S. and Cheng, S.I., "Numerical Solution of the Compressible Navier-Stokes Equations for the Near Wake", Physics of Fluids, Vol. 13, No. 1, 1970, pp. 37-52.

5. Weinbaum, S., "Rapid Expansion of a Expansion of a Supersonic Boundary Layer and its Applications to the Near Wake", AIAA Journal, Vol. 4, No. 2, 1966, pp. 217-226.

6. Osu, H., Abe, T., Ohnishi, Y., Sasoh, A. and Takayama, K., "Numerical Investigation of High Enthalpy Flow Generated by Expansion Tube", AIAA Journal, Vol. 40, No. 12, 2002, pp. 2423-2430.

7. Grasso, F. and Pettinelli, C., "Analysis of Laminar Near Wake Hypersonic Flow", Journal of Spacecraft and Rockets, Vol. 32, No. 6, 1995, pp. 970-980.

8. Tai, C-S. and Kao, A.F., "Navier-Stokes Solver for Hypersonic Flow Over a Slander Cone", Journal of Spacecraft and Rockets, Vol. 31, No. 1, 1994, pp.215-222.

9. Lamb, J.P. and Oberkampf, W.L., "Review and Development of Base Pressure and Base Heating Correlations in Supersonic Flow", Journal of Spacecraft and Rockets, Vol. 32, No. 1, 1995, pp. 8-23.

10. Wood, A.W., Gnoffo, P.A. and Rault, D.F.G., "Aerodynamic Analysis of Commercial Experiment Transport Reentry Capsule", Journal of Spacecraft and Rockets, Vol. 34, No. 5, 1996, pp. 643-646.

11. Teramoto, S., Hiraki, K. and Fujii, K., "Numerical Analysis of Dynamic Stability of a Reentry Capsule at Transonic Speed", AIAA Journal, Vol. 39, No. 4, April 2001, pp. 646-653.

12. Yamamoto, Y. and Yoshioka, M., "CFD and FEM Coupling Analysis of OREX Aero-thermodynamic Flight Data", AIAA 95-2087.

13. Tam, L.T., "LU-SGS Implicit Scheme for Entry Vehicle Flow Computation and Comparison with Aerodynamic Data", AIAA 92-2671 CP, 1992.

14. Liever, P.A., Habchi, S.D., Burnell, S. I. and Lingard, J.S., "Computational Fluid Dynamics Prediction of the Beagle 2 Aerodynamic Data Base", Journal of Spacecraft and Rockets, Vol. 40, No. 5, 2003, pp.632-638.

15. Haas, B.L. and Venkatapathy, E., "Mars Path Finder Computations Including Base Heating Predictions", AIAA 95-2086, 1995.

16. Longo, J.M.A., Orlowski, M. and Bruck., "Considerations of CFD Modeling for the Design of Reentry Vehicle", Aerospace Science Technology, Vol.4, 2000, pp. 337-345.

17. Sietzen, F., "Heir to Apollo: Shaping the CEV, Aerospace America, January 2006, pp. 30- 36.

18. Mehta, R.C., "Computation of Flow Field Over Reentry Capsules at Supersonic Mac h Numbers", Computational Fluid Dynamics Journal, Vol. 13, Oct. 2004, pp. 585-596.

19. Peyret, R. and Viviand, H., "Computational Methods for Fluid Flow", Springer-Verlag, New York, 1993.

20. Jameson, A., Schmidt, W. and Turkel, E., "Numerical Solution of Euler Equations by Finite Volume Methods Using Runge-Kutta Time Stepping Schemes", AIAA 81-1259, 1981.

21. Mehta, R.C., "Numerical Analysis of Aerodynamic Drag Coefficient for Various Reentry Configurations at High Speed", AIAA 2006-3173, 2006.

22. Mehta, R.C., Numerical Simulation of Supersonic Flow Past Reentry Capsules, Shock Waves", DOI 10.1007/s 00193-005-0003-0, 2006.